Decomposition and primary crystallization in undercooled $Zr_{41.2}Ti_{13.8}Cu_{12.5}Ni_{10.0}Be_{22.5}$ melts

R. Busch,[a] S. Schneider, A. Peker, and W. L. Johnson
W. M. Keck Laboratory of Engineering Materials, California Institute of Technology, Pasadena, California 91125

(Received 19 April 1995; accepted for publication 5 July 1995)

$Zr_{41.2}Ti_{13.8}Cu_{12.5}Ni_{10.0}Be_{22.5}$ bulk metallic glasses were prepared by cooling the melt with a rate of about 10 K/s and investigated with respect to their chemical and structural homogeneity by atom probe field ion microscopy and transmission electron microscopy. The measurements on these slowly cooled samples reveal that the alloy exhibits phase separation in the undercooled liquid state. Significant composition fluctuations are found in the Be and Zr concentration but not in the Ti, Cu, and Ni concentration. The decomposed microstructure is compared with the microstructure obtained upon primary crystallization, suggesting that the nucleation during primary crystallization of this bulk glass former is triggered by the preceding diffusion controlled decomposition in the undercooled liquid state. © *1995 American Institute of Physics.*

In the last decade, phase separation in the amorphous or undercooled liquid state has been studied in a large variety of metallic glasses. Decomposition was, for example, reported in the Ti–Zr–Be system,[1,2] in Zr–Cu,[3,4], Zr–Co,[5,6] and lately in the La–Al–Ni[7] and the Zr–Y–Ni–Al[8] bulk metallic glass (BMG) forming systems. In BMG forming alloys, phase separation becomes an important factor in understanding the crystallization process and the glass forming ability.

The novel multicomponent BMG formers that, for example, additionally include Zr–Al–Ni,[9] Zr–Al–Cu–Ni,[10] and Zr–Ti–Cu–Ni–Be,[11] exhibit an extremely high glass forming ability. For the $Zr_{41.2}Ti_{13.8}Cu_{12.5}Ni_{10.0}Be_{22.5}$ alloy, a cooling rate of only 1 K/s is required to suppress crystallization and to form a metallic glass.[12] If one assumes classical nucleation from a homogeneous undercooled liquid state below the melting point or a supercooled liquid state above the glass transition, this implies very small nucleation rates for crystallization at relatively high diffusion constants[13] and should result in a rather coarse microstructure upon crystallization. However, in contradiction to this, there are indications in several BMG forming alloy systems that primary crystallization results in a microstructure consisting of nanocrystals with a very high number density embedded in an amorphous matrix.[14–16] In this letter we will show that the $Zr_{4.12}Ti_{13.8}Cu_{12.5}Ni_{10.0}Be_{22.5}$ alloy decomposes during undercooling in the liquid state. This decomposition appears to be a necessary precursor for the nucleation of crystals and further results in a uniform distribution of crystals on a very fine length scale during primary crystallization. Results of atom probe field ion microscopy (AP/FIM) and transmission electron microscopy (TEM) will be shown to support this description.

Amorphous alloy ingots with a nominal composition of $Zr_{41.2}Ti_{13.8}Cu_{12.5}Ni_{10.0}Be_{22.5}$ were prepared from a mixture of the elements of purity ranging from 99.5% to 99.9% by induction melting on a water-cooled silver boat under a Ti gettered argon atmosphere. Several pieces were remelted together in a $\frac{1}{2}$ inch inner diameter silica tube and then water quenched, resulting in a 4 inch long amorphous cylindrical rod. To produce FIM tips, bars with a square cross section (250×250) μm were cut from the 1/2 inch diameter rod. The samples then were electropolished in a solution of 10% H_3ClO_4 and 90% CH_3COOH at 4–12 V dc to obtain a tip shape. The AP/FIM studies were carried out with the AP/FIM of the Institut für Metallphysik in Göttingen.[17] The specimens were imaged either with a mixture of 15% H_2 and 85% Ne or with pure Ne at 50 K to obtain a phase contrast. The atom probe analyses were performed at 50 K with a ratio of 20% between pulse voltage and permanently applied voltage.

Figure 1(a) shows the FIM image of the center of the slowly cooled amorphous $Zr_{41.2}Ti_{13.8}Cu_{12.5}Ni_{10.0}Be_{22.5}$ rod. It represents a state that was cooled with a rate of approximately 10 K/s. The image gas was a mixture of 85% Ne and 15% H_2 at a total pressure of 6×10^{-4} Pa. The bright spots are the images of single surface atoms in real space. Ring like patterns (poles) resulting from a crystal structure are not observed. However, the imaged atoms are not uniformly distributed, resulting in bright and darker areas corresponding to a higher and lower density of imaged atoms, respectively. This originates from the fact that the radius of the tip changes local. The local radius at the bright regions is

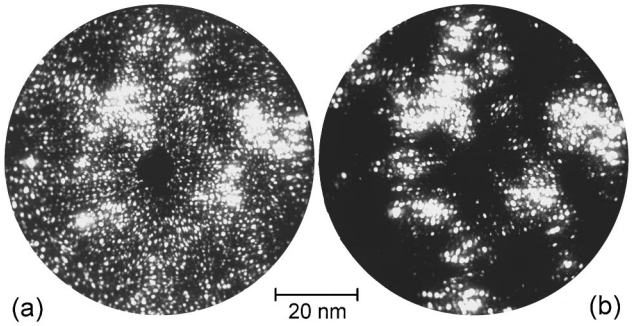

FIG. 1. (a) Field ion micrograph of the center of an amorphous $Zr_{41.2}Ti_{13.8}Cu_{12.5}Ni_{10.0}Be_{22.5}$ sample rod imaged with 85% Ne+15% H_2 at a voltage of 8.2 kV. (b) Field ion micrograph of the same area of the sample imaged with pure Ne at 9.5 kV.

[a]Electronic mail: busch@hyperfine.caltech.edu

 0003-6951/95/67(11)/1544/3/$6.00

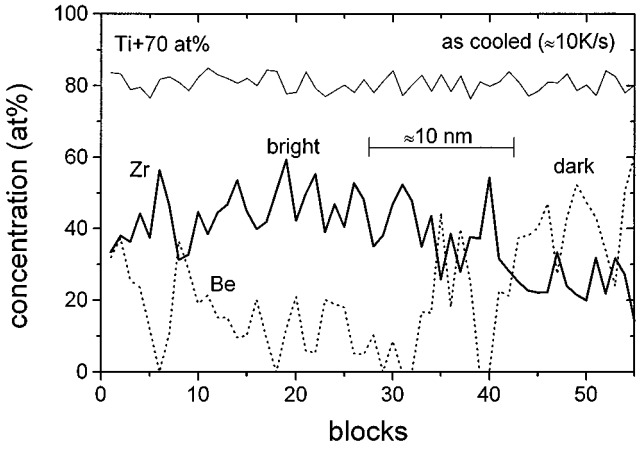

FIG. 2. Atom probe concentration profile from the center of an amorphous $Zr_{41.2}Ti_{13.8}Cu_{12.5}Ni_{10.0}Be_{22.5}$ sample rod. The Zr-rich regions appear bright and the Be-rich regions appear dark on the FIM images.

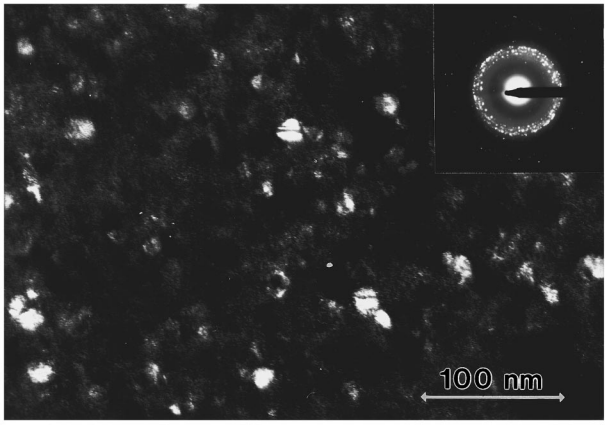

FIG. 3. Dark field TEM image of a $Zr_{41.2}Ti_{13.8}Cu_{12.5}Ni_{10.0}Be_{22.5}$ alloy after primary crystallization.

smaller than at the dark regions. This results in a larger local electric field above bright regions and a higher probability for the imaging gases to be ionized. The reasons for the local changes in tip radius are usually inhomogeneities in the composition of the sample that cause parts of the sample itself to evaporate faster thus producing the observed phase contrast (see, for example, Ref. 18). Since Ne has a higher ionization field compared to H_2, the minimum ionization field increases by removing the H_2 from the chamber. This enhances the phase contrast as demonstrated in Fig. 1(b) where the same part of the sample was solely imaged with neon. Now the field is too low to create a sufficiently high ion flux of the remaining Ne to image the surface atoms above the darkly imaged phase. The typical length scale of the bright and dark regions on this image that can be regarded as a two dimensional projection of a sponge structure is of the order of 50 nm and appears to be rather coarse.

Using the atom probe, composition analyses of the two phases were performed. By using a reflectron detector system[17] we were able to obtain sufficiently high mass resolution to separate all masses of the five components in their respective state of ionization. In averaging over all measurements, we measured 23% of the beryllium expected based on the weight of content in the alloy. Thus, the beryllium has a strong tendency to evaporate preferentially compared to the other components. In the following concentration profile the Be concentration has been corrected for this effect. Figure 2 shows the measured concentrations of Zr, Be, and Ti as a function of the sampling depth. The lateral resolution of this measurement is about 3 nm due to the respective voltage at the tip. The profile shows that the Zr and the Be are not homogeneously distributed in the sample. Regions with a low Be content have a higher Zr concentration and vice versa. By comparing the location of the atom probe hole on the FIM image with the corresponding concentration of the profile, we determined that the bright areas on the FIM images are Zr-rich while the dark regions are Be-rich. Figures 1(a) and 1(b), for example, were taken at the end of the profiling shown in Fig. 2 without tilting the tip. The probe hole, which is located in the center of the dead spot in the middle of the microchannelplate screen [Fig. 1(a)] is found to be above a dark area. The composition fluctuations in the Cu and Ni concentration (not shown) are comparable to the fluctuations observed in the Ti concentration. The measured concentration variations for Ti, Cu, and Ni do not exceed variations expected from counting statistics. They are therefore statistically insignificant in contrast to the fluctuations in the Be and Zr content. Hence, we can conclude that the decomposition involves mainly the Be and Zr concentration.

The decomposition of the $Zr_{41.2}Ti_{13.8}Cu_{12.5}Ni_{10.0}Be_{22.5}$ alloy in the undercooled liquid state leads to an amorphous microstructure with locally different Zr and Be compositions. Thus, the glass transition temperature as well as the temperature for primary crystallization are expected to change locally with the typical length scale of the decomposed microstructure. For the Zr–Ti–Cu–Ni–Be alloy system, it has been shown that the glass transition temperature and the crystallization temperature decrease with increasing Zr concentration.[19,20] This is a general effect found in Zr-based glass formers. For example, this is found in binary systems combining Zr with a late transition metal like Ni, Fe, and Co, it is also observed in ternary and quaternary BMG formers such as Zr–Al–Ni[9] and Zr–Al–Cu–Ni.[10] Hence, the crystallization should preferentially start in the Zr-richer regions [bright in Figs. 1(a) and (b)]. Further the growth of these crystals should be limited to the size of the phase separated domains. This in turn has to lead to nanocrystals which are Zr-rich, embedded in a Be-rich amorphous matrix that is thermally more stable with respect to crystallization. Figure 3 shows the dark field TEM image of an amorphous $Zr_{41.2}Ti_{13.8}Cu_{12.5}Ni_{10.0}Be_{22.5}$ alloy that was reheated into the supercooled liquid region until primary crystallization occurred. The microstructure indeed consists of nanocrystals of a high number density embedded in an amorphous matrix as expected from the preceding decomposition in the undercooled liquid state. Further results of the crystallization process will be published elsewhere.[16]

The occurrence of phase separation in the undercooled liquid state is thermodynamically caused by a miscibility gap that opens up in between two thermodynamically favored undercooled melts that are Be-rich and Zr-rich in our case. Radiative cooling curves of undercooled

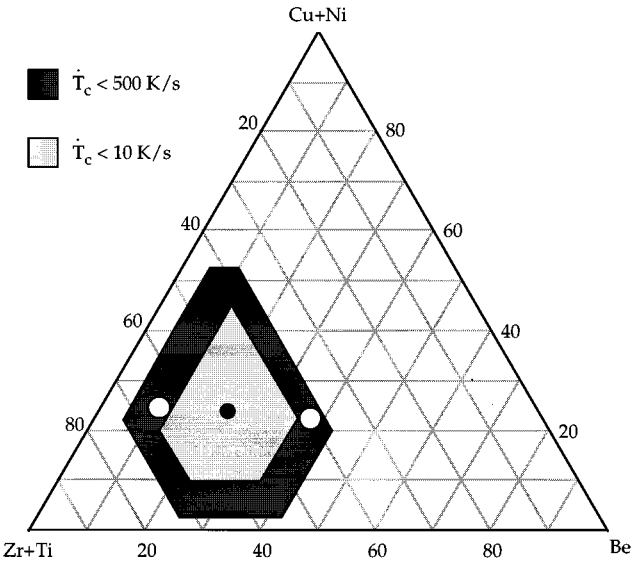

FIG. 4. Quasi-ternary cut through the (Zr–Ti)–(Cu–Ni)–Be phase diagram. The compositions of the initial $Zr_{41.2}Ti_{13.8}Cu_{12.5}Ni_{10.0}Be_{22.5}$ melt (●) and the approximate compositions of the two resulting phases (○) are marked.

$Zr_{41.2}Ti_{13.8}Cu_{12.5}Ni_{10}Be_{22.5}$ melts measured in an electrostatic levitator suggest that the undercooled liquid starts to decompose below about 800 K.[21] This stabilization of different alloy compositions can be attributed to the development of distinct short-range orders for those different compositions of the undercooled liquid. The concentrations of the two phases correspond to the composition limits of the Zr–Ti–Cu–Ni–Be alloys with highest BMG forming ability defined by the critical cooling rate for glass formation. This is visualized in Fig. 4 by a quasiternary cut through the (Zr–Ti)–(Cu–Ni)–Be phase diagram. The region in which the melt requires critical cooling rates, $\dot{T}_c$, of less than 10 K/s to form a bulk metallic glass corresponds to the size of the observed two phase field with respect to its Be and Zr concentration. The decomposition products themselves (○) require much higher cooling rates ($\dot{T}_c$<500 K/s) if they are produced by cooling from the melt. That means both phases themselves are not as good a glass former as the $Zr_{41.2}Ti_{13.8}Cu_{12.5}Ni_{10.0}Be_{22.5}$ with its tendency to phase separation. This suggests that the tendency to phase separation in the undercooled $Zr_{41.2}Ti_{13.8}Cu_{12.5}Ni_{10.0}Be_{22.5}$ melt is a contributing factor to its *extremely* high glass forming ability. It is very likely that, prior to crystallization, the alloy melt has to decompose into a Zr-rich and a Be-rich alloy with different short range orders, which exhibit a higher nucleation probability for the formation of intermetallic compounds compared to the initial homogeneous liquid state. In this picture the decomposition, e.g., proceeding by a spinodal unmixing process is the limiting factor for nucleation of crystalline phases and thus determines the critical cooling rate.

We conclude that the $Zr_{41.2}Ti_{13.8}Cu_{12.5}Ni_{10.0}Be_{22.5}$ undercooled melt decomposes during cooling in the liquid state and forms a two phase mixture of respective Zr-rich and Be-rich amorphous regions with a typical length scale of tens of nanometers for slow cooling rates. On reheating the decomposed alloy, the crystallization starts in the undercooled liquid phase with the lower crystallization temperature. Since Zr-richer Zr–Ti–Cu–Ni–Be alloys are thermally less stable with respect to crystallization than Be-richer alloys, crystallization of the reheated amorphous alloy begins in the Zr-rich portions of the microstructure. The time scale of the observed decomposition in the undercooled liquid state on a fine length scale determines the critical cooling rate and ultimately leads to local primary crystallization with nanocrystallites embedded in an amorphous matrix of different composition. The crystallization most likely also involves the other components Ti, Cu, and Ni. This will be subject to further investigation.

We would like to thank R. Kirchheim for giving us the opportunity to use the AP/FIM in Göttingen, D. Isheim and A. Pundt for their assistance with the AP/FIM, and C. Garland for her assistance with the TEM experiments. This work was supported by the Alexander von Humboldt Foundation via the Feodor Lynen Program and by the U.S. Department of Energy (Grant No. DEFG-03-86ER45242).

[1] L. E. Tanner and R. Ray, Scr. Metall. **14**, 657 (1980).
[2] A. R. Pelton and L. E. Tanner, in *Proceedings of the 5th International Conference on Rapidly Quenched Metals*, edited by S. Steeb and Warlimont (North Holland, Amsterdam, 1985), p. 747; R. Grüne, M. Oehring, R. Wagner, and P. Haasen, *ibid.* p. 761.
[3] D. Deng and A. S. Argon, Acta Metall. **10**, 2011 (1986).
[4] R. Bormann, F. Gärtner, and F. Haider, Mater. Sci. Eng. **97**, 79 (1988).
[5] F. Gärtner, Ph.D. thesis, University of Göttingen (1992).
[6] R. Busch, F. Gärtner, S. Schneider, R. Bormann, and P. Haasen, Mater. Res. Soc. Symp. Proc. **343**, 229 (1994).
[7] A. H. Okumura, A. Inoue, and T. Masumoto, Acta Metall. Mater. **41**, 915 (1993).
[8] K. Sugiyama, A. H. Shinohara, Y. Waseda, S. Chen, and A. Inoue, Mater. Trans. Jpn. Inst. Metals **35**, 481 (1994).
[9] A. Inoue, T. Zhang, and T. Masumoto, Mater. Trans. JIM **31**, 177 (1990).
[10] T. Zhang, A. Inoue, and T. Masumoto, Mater. Trans. JIM **32**, 1005 (1991).
[11] A. Peker and W. L. Johnson, Appl. Phys. Lett. **63**, 2342 (1993).
[12] Y. J. Kim, R. Busch, W. L. Johnson, A. J. Rulison, and W. K. Rhim, Appl. Phys. Lett. **65**, 2136 (1994).
[13] U. Geyer, S. Schneider, W. L. Johnson, Y. Qiu, T. A. Tombrello, and M. P. Macht, Phys. Rev. Lett. (to be published).
[14] Y. H. Kim, A. Inoue, and T. Masumoto, Mater. Trans. JIM **31**, 749 (1990).
[15] W. Liu and W. L. Johnson (unpublished research).
[16] S. Schneider, R. Busch, and W. L. Johnson (unpublished research).
[17] G. P. Geber, T. Al-Kassab, D. Isheim, R. Busch, and P. Haasen, Z. Metallkde. **83**, 449 (1992).
[18] M. K. Miller and G. D. W. Smith, *Atom Probe Microanalysis: Principles and Applications to Materials Problems* (MRS, Pittsburgh, 1989).
[19] W. L. Johnson and A. Peker, in *Proceedings of the NATO Advanced Research Workshop on Science and Technology of Rapid Solidification and Processing*, West Point Military Academy, June 21–24, 1994, edited by Monde A. Otooni (Kluwer Academic, Dordrecht, 1994), p. 25.
[20] A. Peker, Ph.D. thesis, California Institute of Technology (1994).
[21] R. Busch, Y. J. Kim, W. L. Johnson, A. J. Rulison, W. K. Rhim, and D. Isheim, Appl. Phys. Lett. **66**, 3111 (1995).